ACS OMEGA

http://pubs.acs.org/journal/acsodf

Article

# Hydrogen Evolution from Additive-Free Formic Acid Dehydrogenation Using Weakly Basic Resin-Supported Pd Catalyst

Lichun Li,* Xiangcan Chen, Cheng Zhang, Geshan Zhang, and Zongjian Liu*

Cite This: *ACS Omega* 2022, 7, 14944−14951

Read Online

ACCESS | Metrics & More | Article Recommendations | Supporting Information

**ABSTRACT:** Hydrogen, as a noncarbon energy source, plays a significant role in future clean energy vectors. However, concerns about the safe storage and transportation of hydrogen gas limit its wide application. Featured with high $H_2$ volumetric density, nontoxicity, and nonflammability, formic acid (FA) is regarded as one of the most encouraging chemical hydrogen carriers. The search for heterogeneous catalysts with decent catalytic activity and stability for FA decomposition is one of the hottest research topics in this area. In this paper, three weakly basic resins with different functional groups, including D201 with $-N^+(CH_3)_3$, D301 with $-N(CH_3)_2$, and D311 with $-NH_2$, were investigated as alternative catalyst supports for Pd catalysts. The prepared basic resin-supported Pd catalysts were evaluated for the FA dehydrogenation reaction under atmospheric pressure and temperatures ranging from 30 to 70 °C. The results showed that the catalytic activity of the three different resin-supported Pd catalysts follows the order of Pd/D201 > Pd/D301 > Pd/D311. Particularly, a high turnover frequency value of 547.6 $h^{-1}$ was achieved when employing Pd/D201 as the FA dehydrogenation reaction catalyst at 50 °C. The apparent activation energies for the three different Pd/resin catalysts were calculated, of which the Pd/D210 catalyst demonstrates the lowest activation energy of 42.9 kJ $mol^{-1}$. The reasons for the superior catalytic behavior, together with the reaction mechanism, were then investigated and illustrated.

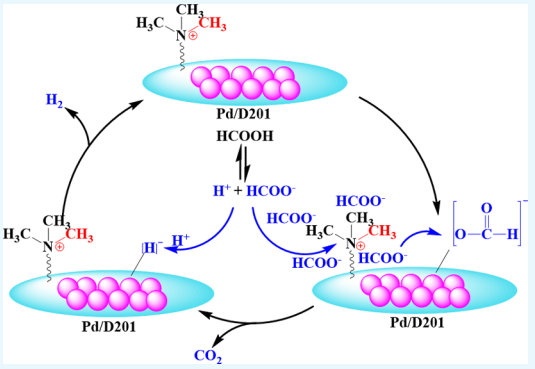


## 1. INTRODUCTION

The excessive amount of greenhouse gas $CO_2$ released from conventional fossil fuel combustions has a negative impact on global climate change; hence, the search for a clean $CO_2$-netural alternative energy source is of great importance to the human society.[1,2] Hydrogen is a potential clean energy substitute as water is the only product when it is combusted for energy purpose.[3,4] However, due to the low volumetric density of $H_2$ (0.08988 g/L at room temperature and atmospheric pressure), its storage and transportation is often associated with handling pressurized gas containers.[5] Thus, safe and cost-effective storage and transportation remain as the two major challenges blocking the utilization of hydrogen as the energy source in large scale.[6−8] Chemical hydrogen carriers offer a unique way to store hydrogen energy in chemical compounds and transport hydrogen in the form of hydrogen-rich molecules. Metal hydrides and their alloys, ammonia, methanol, and formic acid (FA) have been explored as promising chemical hydrogen carriers.[9−14] Among these, FA is present in the form of liquid at room temperature and is featured with properties like high gravimetric (4.4 wt %) and volumetric (53 g $H_2$ $L^{-1}$) densities, nonflammability, and low toxicity and hence is considered as one of the most promising candidates as a chemical hydrogen carrier. Therefore, the development of a sustainable catalytic system for the on-site production of hydrogen from FA is of great importance and has raised considerable amount of research attention.

Generally, the on-site production of hydrogen from FA can be achieved at atmospheric pressure and relatively low reacting temperatures of 20−80 °C in the presence of a proper catalyst. It is well accepted that FA decomposition can occur through dehydrogenation (eq 1) and dehydration (eq 2) pathways, depending on the reaction conditions and catalyst properties.[15,16]

$$HCOOH \leftrightarrow CO_2 + H_2 \quad \Delta G = -48.4 \text{ kJ mol}^{-1} \tag{1}$$

$$HCOOH \leftrightarrow CO + H_2O \quad \Delta G = -28.5 \text{ kJ mol}^{-1} \tag{2}$$

Accordingly, the dehydration reaction of FA is the main side reaction that needs to be minimized to boost the efficiency of the desired dehydrogenation reaction to produce hydrogen on-site. With the distinguished advantages of easy separation and reusability, the application and rational design of heteroge-

Received: January 29, 2022
Accepted: April 5, 2022
Published: April 20, 2022

neous catalysts for FA have been reported intensively in recent years. In particular, the application of supported Pd nanoparticle (NP) catalysts has gained substantial research attention owing to their ability to tolerate CO and their extraordinary catalytic performance toward conversion and selectivity regarding $H_2$ production from FA decomposition under moderate temperatures.[15−20] The utilization of Pd-based heterogeneous catalysts in the FA decomposition process is often accompanied with nearly 100% selectivity toward the FA dehydrogenation reaction. For example, as reported in the open literature, no trace of CO was detected when using Pd/C[21] and Pd-CNTs[22] as catalysts for FA decomposition, while less than 5 ppm of CO was detected when using Pd/resin (IRA96SB) as the catalyst.[23]

In order to achieve better catalytic activity and stability, alloying with another metal was often employed as an effective approach as it can successfully modify the electronic and geometric framework of the active Pd metal. This approach was intensively demonstrated in the open literature, with improved catalytic performance demonstrated by PdAu,[24,25] PdAg,[18,26−28] PdCo,[29] PdNiAg,[30] PdCu,[31] PdIr,[32] IrPdAu,[33] and PdCoAu[34] alloy catalysts. Another effective approach to improve the catalytic performance of single Pd-based catalysts is to vary the support materials for Pd catalysts. For supported catalysts, the physiochemical properties of the support are highly associated with the catalytic performance of the catalysts as they often affect the dispersion of the active metal, the stability of the active metal, and sometimes the chemical state of the active metal. Hence, a large variety of materials have been investigated as catalyst supports for Pd-based heterogenous catalysts, including carbon materials,[35,36] graphene oxide,[27] MOFs,[15] metal oxides,[37] macroreticular resins,[23,31] and so on. Among these, the application of macroreticular basic resins was proven to be one of the promising options for catalyst support as the weakly basic $-N(CH_3)_2$ groups within the resin facilitate the decomposition of the O−H bond in HCOOH, hence improving the activity for FA dehydrogenation.[31]

However, investigations of other weakly basic resins with different functional groups as supports for the Pd catalyst in the FA dehydrogenation reaction are rarely reported in the open literature. Therefore, in the current paper, three weakly basic resins with different functional groups, including D201 with $-N^+(CH_3)_3$, D301 with $-N(CH_3)_2$, and D311 with $-NH_2$, were investigated as alternative catalyst supports for Pd catalysts for their catalytic performance in the FA dehydrogenation process. The selected three different functional groups are typical representatives of quaternary amine, tertiary amine, and primary amine. To point out, the additive-free FA decomposition reaction process was employed in the current paper as additives like HCOONa would decrease the $H_2$ storage potential. In addition, several physiochemical characterization methods were employed to rationalize the difference in the catalytic performance of the three Pd/resin catalysts toward the FA dehydrogenation reaction. Furthermore, the catalytic reaction mechanism of FA dehydrogenation in the presence of Pd/resin catalysts with different functional groups was proposed and illustrated.

## 2. EXPERIMENTAL SECTION

**2.1. Catalyst Preparation.** *2.1.1. Resin Pretreatment.* The purchased resins including D201, D301, and D311 were first washed repeatedly with distilled water until the filtrates become colorless and clear. Then, the resin was immersed in a series of solutions including 1.0 mol/L $HNO_3$, 1.0 mol/L NaOH, and 1.0 mol/L $KNO_3$. The time for immersion of the resin is 12 h for each solution. After soaking, the resin was rinsed with distilled water several times until the filtrate was neutral. Finally, the resin support was obtained after vacuum drying at 80 °C for 12 h.

*2.1.2. Preparation of the Pd/Resin Catalyst.* Before the deposition, the pretreated resin was grinded to achieve a sample size less than 0.1 mm. The grinded resin (0.5 g) was then mixed with an aqueous solution containing 20 mL of water and 1.25 mL of 2 mg Pd/mL $PdCl_2$ solution. The mixture was then stirred at room temperature for 24 h before filtration. The solid obtained from filtration was washed repeatedly with distilled water. Subsequently, the samples were transferred into 50 mL of distilled water and pre-reduced with 15 mL of 1 M $NaBH_4$. After the reaction, the catalyst was vacuum-dried at 80 °C for 12 h after being filtered and washed repeatedly with distilled water. The attained sample was labeled as the Pd/resin catalyst. Pd loading was controlled at 0.5 wt % for all catalyst samples. Inductively coupled plasma optical emission spectrometry (ICP-OES) was conducted to obtain the actual Pd loading in the Pd/resin catalysts. The actual Pd content falls in the range of ±10% of the intended Pd loading of 0.5 wt %, which indicates the easy attachment of Pd onto the resin support.

**2.2. Catalyst Characterization.** The transmission electron microscopy (TEM) images of all tested catalyst samples were acquired on a JEOL JEM-1200EX electron microscope operated at 200 kV. All samples were gold-plated before acquiring the TEM images to increase their conductivity for measuring purposes. The BET surface area and pore structure were attained from the $N_2$ adsorption/desorption measurement on a Quantachrome Autosorb-IQ instrument in static measurement mode at −196 °C. All samples were degassed at 200 °C for 5 h prior to measurements. X-ray photoelectron spectroscopy (XPS) measurements were conducted on an ESCALAB 250XI spectrometer with 24.2 W of Al K$\alpha$ radiation. ICP-OES was conducted on a Thermo Fisher iCAP PRO system to obtain the actual Pd loading in the Pd/resin catalysts.

**2.3. Hydrogen Generation from Formic Acid Dehydrogenation.** FA dehydrogenation in aqueous solutions were performed in a round-bottom flask containing 50 mg catalyst and 5 mL of 0.25 M FA solution. A water bath with magnetic stirring is employed to control the reaction temperature and apply magnetic stirring to the reaction medium. The speed of the applied magnetic stirring is maintained at about 850 rpm. The catalyst was added into the round-bottom flask prior to the addition of FA solution. The addition of 5 mL of 0.25 M FA solution initiates the dehydrogenation reaction, and the corresponding evolved gas was monitored by a gas burette system. To point out, the water level at the exhaust side of the gas burette was always kept as the same level to the inside to eliminate the pressure difference. The evolved gases were analyzed using a GC-1690 instrument equipped with a thermal conductivity detector (TCD) and a TDX-1 column. No trace of CO was detected during the FA decomposition reaction in the presence of all three prepared Pd/resin catalysts (Pd/D201, Pd/D301, and Pd/D311) which suggests a ∼100% selectivity toward FA dehydrogenation.

The FA conversion rate was calculated according to eq 3



https://doi.org/10.1021/acsomega.2c00601
ACS Omega 2022, 7, 14944−14951

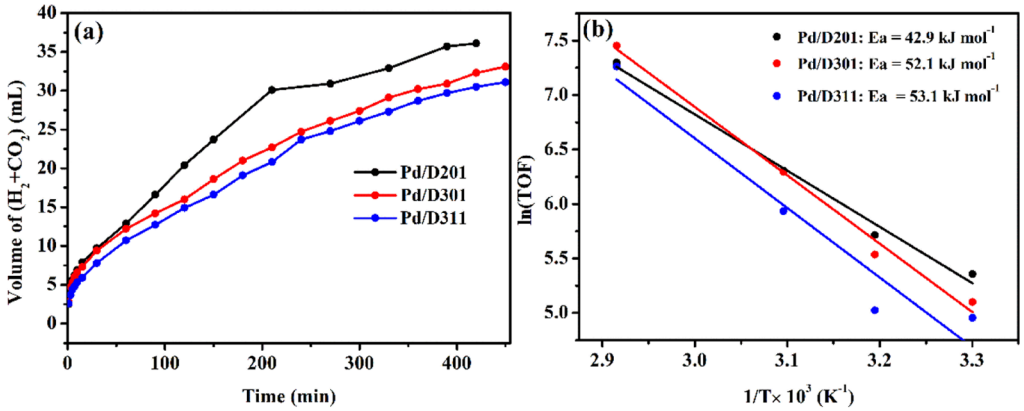


**Figure 1.** (a) Volume of gas evolved from FA dehydrogenation as a function of time in the presence of Pd/D201, Pd/D301, and Pd/D311 catalysts. Reaction conditions: 50 °C and 5 mL of 0.25 M HCOOH solution; (b) Arrhenius plot of TOF at 5 min as a function of reacting temperatures, together with the calculated $E_a$ values of Pd/D201, Pd/D301, and Pd/D311 catalysts in the temperature range of 30−70 °C.

**Table 1. Catalytic Performance of Supported Pd Heterogeneous Catalysts Toward HCOOH Dehydrogenation in Aqueous Solution Without Additives**[b]

| catalysts | metal loading | reaction conditions | $T$ (°C) | conversion (%) | $TOF_{initial}$ ($h^{-1}$) | $E_a$ (kJ $mol^{-1}$) | eef |
|---|---|---|---|---|---|---|---|
| Pd/D201 | 0.5 | 0.05 g cat, 0.25 M FA, 5 mL, 150 min | 50 | 38.8 | 547.6[a] | 42.9 | this work |
| Pd/D301 | 0.5 | 0.05 g cat, 0.25 M FA, 5 mL, 150 min | 50 | 30.4 | 541.7[a] | 52.1 | this work |
| Pd/D311 | 0.5 | 0.05 g cat, 0.25 M FA, 5 mL, 150 min | 50 | 27.2 | 445.3[a] | 53.1 | this work |
| Pd/C | 10 | 0.10 g cat, 1.33−4.00 M FA, 70 mL, 300 min | 50 | | 186−347[c] | 53.7 | 36 |
| Pd/C | 10 | 0.025 g cat, 6 M FA, 20 mL, 150 min | 50 | 3 | 87 | | 38 |
| Pd/C | 10 | 0.025 g cat, 1 M FA, 10 mL, 120 min | 45 | 40 | 361 | | 39 |
| Pd*$CeO_2$ | 10 | 0.5 M FA, 10 mL | 40 | | 807.7 | 43.02 | 37 |
| Pd/C | 1 | 0.027 g cat, 0.5 M FA, 10 mL, 150 min | 30 | 9 | 240 | | 35 |
| Pd/CNF | 1 | 0.027 g. cat, 0.5 M FA, 10 mL, 150 min | 30 | | 979.1 | 26.2 | 35 |
| Pd/SBA-15-PA | 4.3 | 0.046 g cat, 1.0 M FA, 10 mL | 26 | | 355 | | 40 |
| Pd/C | 1 | 0.50 g cat, 1 M FA, 10 mL, 150 min | 23 | 2 | 38 | | 41 |
| Pd/mpg-$C_3N_4$ | 10 | 0.025 g. cat, 1 M FA, 10 mL, 120 min | 25 | | 144 | 29.1 | 42 |
| Pd/CN | 10 | 0.04 g cat, 1 M FA, 5 mL, | 25 | | 752 | | 43 |
| Pd/SBA-15-$NH_2$ | 10 | 0.5 M FA, 5 mL | 25 | | 481 | 53.01 | 44 |

[a]TOF calculated after 5 min. [b]TOF calculated at FA conversion of 20%. [c]TOF calculated using moles of Pd exposed on the surface after 10 min with HCOOH concentrations of 1.33−4.00 M.

$$x_{FA} = \frac{P_{atm}V_{gas}/RT}{2n} \quad (3)$$

where $P_{atm}$ is the atmospheric pressure (101.325 kPa), $V_{gas}$ is the volume of the generated gases ($H_2$ + $CO_2$) in L, $R$ represents the universal gas constant (8.3145 $m^3$ Pa $mol^{-1}$ K), $T$ represents room temperature (K), and $n$ represents the mole number of FA in the aqueous solution. The turnover frequency (TOF) values at different times are calculated based on eq 4

$$TOF_t = \frac{P_{atm}V_{gas}/RT}{2n_{Pd}t} \quad (4)$$

where $n_{Pd}$ represents the number of Pd molecules used and $t$ represents the reaction time (h).

## 3. RESULTS AND DISCUSSION

The catalytic activities in the form of gas evolved from FA dehydrogenation at 50 °C and atmospheric pressure in the presence of the resin-supported catalysts including Pd/D201, Pd/D301, and Pd/D311 are illustrated in Figure 1a. As can be observed from Figure 1a, the catalytic activity of the three different resin-supported Pd catalysts follows the order of Pd/D201 > Pd/D301 > Pd/D311. Different catalytic performances likely originated from the different functional groups existing on the surface of the tested resins. To point out, the different functional groups $-N^+(CH_3)_3$, $-N(CH_3)_2$, and $-NH_2$ on the surface of D201, D301, and D311 are believed to be the main reason accounting for the significant difference in the catalytic performance toward hydrogen generation from FA dehydrogenation. The effect of temperature on the catalytic decomposition of FA was also evaluated in the temperature range of 30−70 °C, and it was demonstrated that promoted catalytic activity was achieved with the evaluated temperatures for all the three tested Pd/resin catalysts. The results can be found in Figure S1(a−c), Supporting Information. Moreover, the best performed Pd/D201 was recycled and reused for FA dehydrogenation after filtration, water wash, and vacuum drying at 80 °C for 12 h. There is only a minor reduction in the catalytic performance using recycled Pd/D201 even at the fourth run of the FA dehydrogenation reaction (Figure S2, Supporting Information). This proves the decent stability of the Pd/D201 catalyst and hence its potential for practical uses. The Arrhenius plot between the reaction temperature (30−70 °C) and TOF at 5 min, together with the calculated apparent activation energy ($E_a$) of the three tested Pd/Resin catalysts, is presented in Figure 1b.



https://doi.org/10.1021/acsomega.2c00601
ACS Omega 2022, 7, 14944−14951

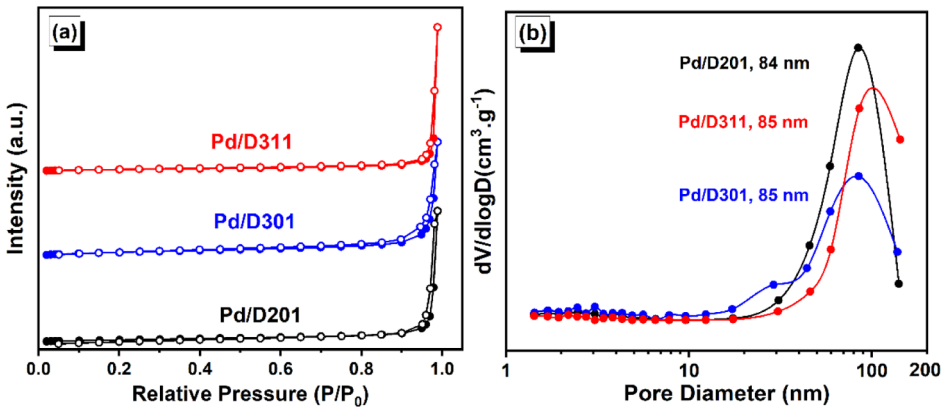


**Figure 2.** $N_2$ adsorption−desorption isotherms (a) and pore size distribution (b) of the catalysts of Pd/D201, Pd/D301, and Pd/D311.

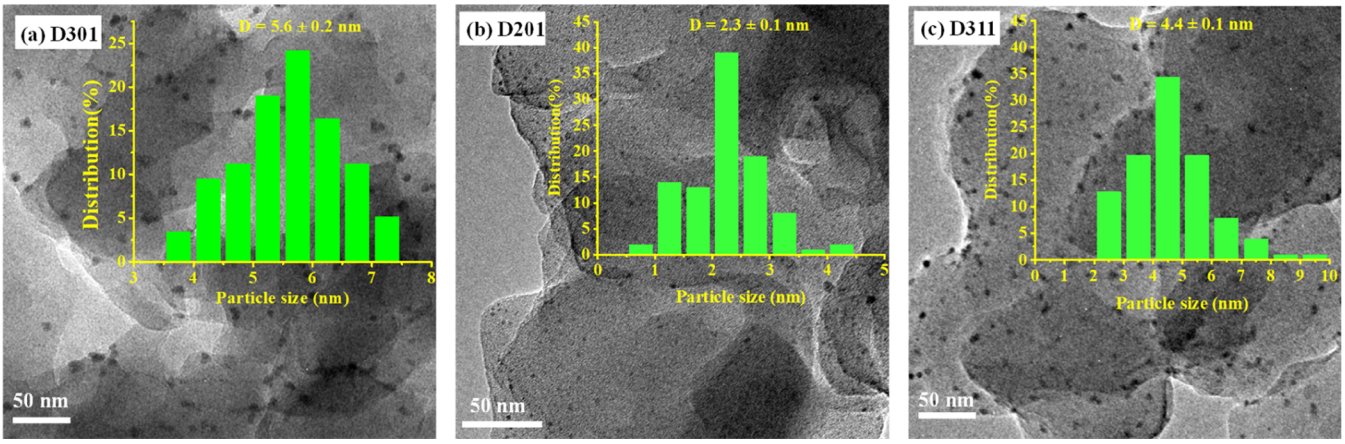


**Figure 3.** TEM images together with the histograms of particle size distributions for the catalysts of Pd/D301 (a), Pd/D201 (b), and Pd/D311 (c).

As expected, the TOF values decreased with the decrease in the reaction temperature for all the tested Pd/resin catalysts. The calculated $E_a$ values for the three catalysts follow the order of Pd/D201 (42.9 kJ $mol^{-1}$) < Pd/D301 (52.1 kJ $mol^{-1}$) < Pd/D311 (53.1 kJ $mol^{-1}$). This observation agrees very well with the catalytic performance of the Pd/resin catalysts demonstrated in Figure 1a. Among these, Pd/D201, with the best catalytic activity toward FA decomposition, has the lowest $E_a$ value of 42.9 kJ $mol^{-1}$. By examining the different $E_a$ values, it is therefore implied that different reaction mechanisms might be involved when employing the different Pd/resin catalysts in the FA decomposition reaction.

Although, it is rather difficult to compare with the literature-published data because of the discrepancy in reaction conditions, the conversion rate at 150 min, initial TOF values, and the calculated $E_a$ values were collected and compared with several published studies in Table 1. When comparing the catalytic activity of our catalyst with the literature-reported catalysts, the selection of the literature data focuses on the mono Pd-based catalysts and those catalytic activity data evaluated without additives (such as HCOONa) in the FA dehydrogenation process. The overall conversion scattered between 2 and 40%, making our best catalyst Pd/D201 as an encouraging choice, with about 38.8% conversion rate at 50 °C in 150 min time span. The apparent activation energy of 42.9−53.1 kJ $mol^{-1}$ is consistent with the literature results which range from 26.2 to 53.7 kJ $mol^{-1}$. Certainly, the Pd/D201 catalyst sits within one of the best performed catalysts when comparing the obtained TOF values with the literature-published data in Table 1.

Therefore, to investigate the fundamental reasons for the different catalytic performances of the three synthesized Pd/resin catalysts, the texture properties of the three as-prepared catalysts were first measured. The obtained $N_2$ adsorption−desorption isotherms and pore size distribution of the three catalysts of Pd/D201, Pd/D301, and Pd/D311 are shown in Figure 2.

As illustrated in Figure 2a, all three samples fall in the classification of type II adsorption isotherms, which indicates the existence of macroporous structures. This was confirmed with the pore size distribution in Figure 2b, with pore sizes of 84, 85, and 85 nm for Pd/D201, Pd/D301, and Pd/D311 catalysts, respectively. The surface areas of the three catalysts including Pd/D201 (15 $m^2$ $g^{-1}$), Pd/D301 (25 $m^2$ $g^{-1}$), and Pd/D311 (11 $m^2$ $g^{-1}$) are within the same magnitude. Compared with the other supports for Pd catalysts such as activated carbon with surface areas of a few hundred square meters per gram, the minor difference in the surface areas of the three resin supports is believed not to make a significant difference on the catalytic performance. Hence, the texture properties of the three catalysts are probably not the main properties that affect the catalytic performance of the supported Pd/resin catalysts in our study.

As reported in previous publications, the particle size of Pd NPs is believed to be one of the key factors influencing the catalytic performance of the supported monometallic Pd catalysts, and a particle size effect is often observed.[38,45,46] It



https://doi.org/10.1021/acsomega.2c00601
ACS Omega 2022, 7, 14944−14951

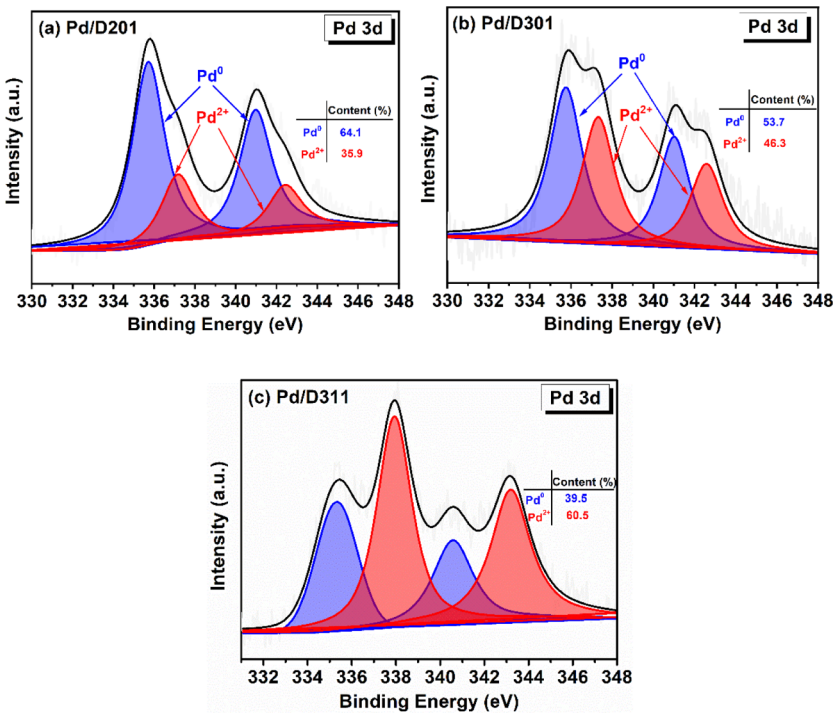


**Figure 4.** XPS spectra of the Pd 3d region for the Pd/D201 (a), Pd/D301 (b), and Pd/D311 (c) catalysts.

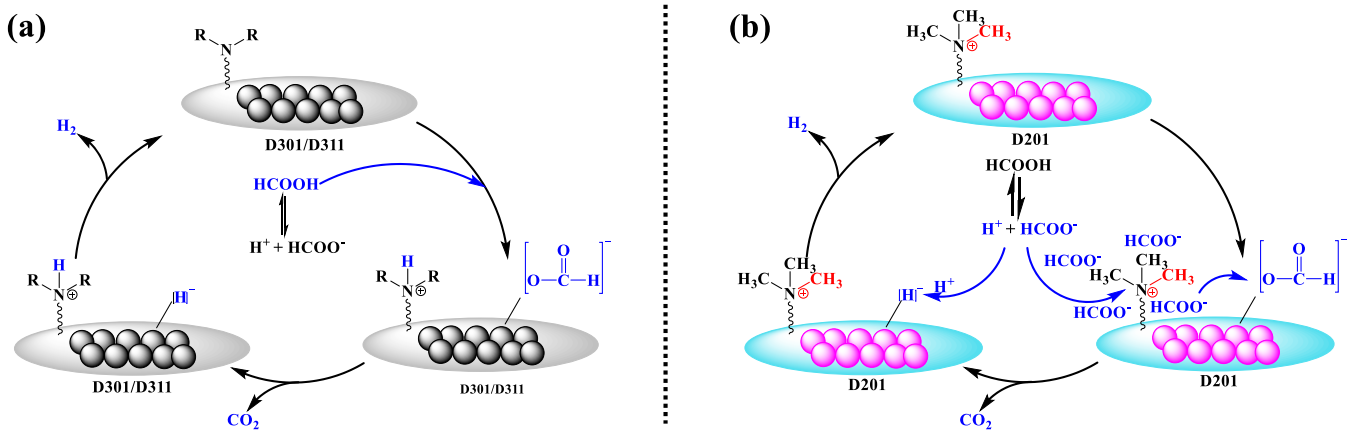


**Figure 5.** Schematic illustration of the proposed reaction mechanisms of the FA dehydrogenation reaction in the presence of Pd/D301 and Pd/D311 catalysts (a) and Pd/D201 catalyst (b).

is believed that supported Pd catalysts with particle sizes larger than 4 nm and very small particle sizes generally result in poor catalytic performance in the FA dehydrogenation reaction process.[18,47] The optimized particle size was then suggested to be within the range of 1.8−3.5 nm.[36] Therefore, the TEM images of the three as-prepared Pd/Resin catalysts were then measured to investigate the effect of Pd NP size on the catalytic performance of FA dehydrogenation. The TEM images, together with the Pd size distribution diagrams of the three as-prepared Pd/resin catalysts, are shown in Figure 3.

As can be seen from Figure 3b, the distribution of Pd NPs is uniform on the surface of the D201 resin, and the resultant average size of Pd NPs is about 2.3 nm, which lies within the optimized particle size range. This agrees with the superior catalytic performance of the Pd/D201 catalyst observed in Figure 3a. On the other hand, the average particle sizes of Pd/D301 and Pd/D311 samples are observed to be ∼5.6 and ∼4.4 nm, respectively. These particles are believed to be too large to generate a decent catalytic performance, which agrees well with the relatively poor catalytic activity in Figure 3 of Pd/D301 and Pd/D311 catalysts. It thus can be concluded that the decent Pd NP size obtained in the Pd/D201 catalyst is certainly beneficial to the superior catalytic performance toward the FA dehydrogenation reaction.

To further explore the possible reaction mechanism, XPS spectra of the Resin-supported catalysts were then measured to investigate the chemical state of Pd NPs on the surface of the catalysts of Pd/D201, Pd/D301, and Pd/D311. The obtained XPS spectra are shown in Figure 4.

To examine the chemical state of Pd on the catalyst surface, the XPS spectra of the Pd 3d region for the Pd/D201, Pd/D301, and Pd/D311 catalysts were measured and presented in Figure 4. As shown in Figure 4, there are two main doublets that exist for all the three tested catalysts, suggesting two different chemical states of Pd. The corresponding peaks assigned to $Pd^0$ and $Pd^{2+}$ are indicated in Figure 4. The peak



https://doi.org/10.1021/acsomega.2c00601
ACS Omega 2022, 7, 14944−14951

area of those peaks was then employed in peak deconvolution analysis to obtain the content of $Pd^0$ and $Pd^{2+}$ in each catalyst. As demonstrated in Figure 4, surface Pd was partially reduced into metallic $Pd^0$ for all the tested catalysts. In addition, the content of $Pd^0$ in the three tested catalysts follows the trend of Pd/D201 > Pd/D301 > Pd/D311, which agrees well with the catalytic performance observed in Figure 1a. Therefore, compared with the functional groups of $-N(CH_3)_2$ and $-NH_2$, the existence of surface functional groups of $-N^+(CH_3)_3$ is more beneficial for the reduction of $Pd^{2+}$ into metallic $Pd^0$, which is considered to be the actual active site for FA dehydrogenation.

Based on the characterization of the physiochemical properties, the reaction mechanism of FA decomposition in the presence of different resin-supported Pd catalysts is therefore proposed and illustrated in Figure 5. It is generally accepted that the reaction mechanism of the FA dehydrogenation reaction involves two potential reaction pathways, including pathway I (i.e., formate anion dehydrogenation pathway)[48,49] and pathway II (i.e., FA dehydrogenation pathway).[50] Naturally, the FA deprotonation reaction is equilibrated in the FA solution, with both HCOOH and $HCOO^-$ that can possibly serve as reacting substances for hydrogen production.[28,40] For Pd/D301 and Pd/D311 catalysts, the surface basic functional group is $-N(R)_2$, where R represents $CH_3$ for D301 and H for D311. As shown in Figure 5a, in the presence of Pd/D301 and Pd/D311 catalysts, FA dehydrogenation mainly uses HCOOH as the starting substance. First, the reaction is initiated by the adsorption of HCOOH, where the $-N(R)_2$ group serves as a proton scavenger and facilitates the deprotonation of HCOOH. Second, the deprotonation product $HCOO^-$ was then adsorbed on the surface of Pd NPs, followed by $\beta$-hydride elimination to produce $CO_2$ and a surface palladium hydride species. Third, the hydride species react with the nearby $-NH^+(R)_2$ species and form $H_2$, together with the regeneration of active $Pd^0$ NPs.

However, for the Pd/D201 catalyst (Figure 5b), FA dehydrogenation mainly uses $HCOO^-$ as the starting substance. First, the reaction is initiated via the absorption of $HCOO^-$ species to the surface of the catalyst through electrostatic interaction with the positively charged $-N^+(CH_3)_3$ group and migration to the nearby Pd NP surface. Second, the formation of $CO_2$ and palladium hydride species was achieved via the $\beta$-hydride elimination of $HCOO^-$. Third, the surface palladium hydride species reacted with the proton in the aqueous solution to form $H_2$ along with $Pd^0$ active site regeneration. To point out, the electrostatic interaction between the positively charged $-N^+(CH_3)_3$ group and $HCOO^-$ species is likely to cause an increasing localized concentration of $HCOO^-$, which boosts the deprotonation of HCOOH and promotes the overall catalytic FA dehydrogenation process. Hence, Pd/D201 catalyst is believed to be a promising candidate for the catalytic FA dehydrogenation reaction process.

## 4. CONCLUSIONS

In the current paper, monometallic Pd catalysts supported on three weakly basic resins with different functional groups, including D201 ($-N^+(CH_3)_3$), D301 ($-N(CH_3)_2$), and D311 ($-NH_2$), were prepared and evaluated as catalysts for the FA dehydrogenation reaction. Different catalytic performances were observed when employing the three different resin-supported Pd catalysts, with Pd/D201 demonstrating best catalytic activity towards the FA dehydrogenation reaction. The corresponding characterizations of the physiochemical properties of the three Pd/resin catalysts revealed that the proper Pd NP size and large content of metallic $Pd^0$ on the catalyst surface are the beneficial properties for achieving a decent catalytic performance in FA dehydrogenation reactions. The different reaction mechanisms of FA dehydrogenation in the presence of Pd/D201, Pd/D301, and Pd/D311 were proposed as well. It was revealed that the superior catalytic performance of Pd/D201 can be explained by the surface positively charged functional group of $-N^+(CH_3)_3$ electrostatically interacting with the negatively charged $HCOO^-$ and causing an increase in the localized $HCOO^-$ concentration. This is likely to boost the deprotonation of HCOOH in aqueous phase and hence result in an improved catalytic performance of Pd/D201 in the overall HCOOH dehydrogenation reaction process.

## ■ ASSOCIATED CONTENT

### Supporting Information

The Supporting Information is available free of charge at https://pubs.acs.org/doi/10.1021/acsomega.2c00601.

Catalytic decomposition of FA at different temperatures of 30−70 °C in the presence of all three tested Pd/resin catalysts and catalytic performance of FA dehydrogenation of four repeated runs in the presence of Pd/D201 catalyst (PDF)

## ■ AUTHOR INFORMATION


### Corresponding Authors

**Lichun Li** − *College of Chemical Engineering, Zhejiang University of Technology, Hangzhou 310014, PR China*; orcid.org/0000-0002-5352-8728; Email: lichunli@zjut.edu.cn

**Zongjian Liu** − *College of Chemical Engineering, Zhejiang University of Technology, Hangzhou 310014, PR China*; Email: zjliu@zjut.edu.cn

### Authors

**Xiangcan Chen** − *College of Chemical Engineering, Zhejiang University of Technology, Hangzhou 310014, PR China*

**Cheng Zhang** − *College of Chemical Engineering, Zhejiang University of Technology, Hangzhou 310014, PR China*

**Geshan Zhang** − *College of Chemical Engineering, Zhejiang University of Technology, Hangzhou 310014, PR China*

Complete contact information is available at: https://pubs.acs.org/10.1021/acsomega.2c00601


### Notes

The authors declare no competing financial interest.

## ■ ACKNOWLEDGMENTS

The work was financially supported by Technology Innovation Center for Land Spatial Eco-restoration in Metropolitan Area, Ministry of Natural Resources and the Fundamental Research Funds for the Central Universities (CXZX2021A02).

## ■ REFERENCES

(1) Gao, R.; Yu, M.; Xu, H.; Li, L.; Deng, M.; Wu, Y.; Chen, Z. Open-Structured Oxyfluorinated Titanium Phosphate Nanosheets Synthesized with the Assistance of an Ionic Liquid and Their Use as

an Anode in Lithium-Ion Batteries. *Energy Fuels* **2021**, *35*, 15213−15222.
(2) Gao, R.; Deng, M.; Yan, Q.; Fang, Z.; Li, L.; Shen, H.; Chen, Z. Structural Variations of Metal Oxide-Based Electrocatalysts for Oxygen Evolution Reaction. *Small Methods* **2021**, *5*, 2100834.
(3) Thomas, J. M.; Edwards, P. P.; Dobson, P. J.; Owen, G. P. Decarbonising energy: The developing international activity in hydrogen technologies and fuel cells. *J. Energy Chem.* **2020**, *51*, 405−415.
(4) Singh, R.; Singh, M.; Gautam, S. Hydrogen economy, energy, and liquid organic carriers for its mobility. *Mater. Today: Proc.* **2021**, *46*, 5420−5427.
(5) Saxena, R. C.; Seal, D.; Kumar, S.; Goyal, H. B. Thermochemical routes for hydrogen rich gas from biomass: A review. *Renewable Sustainable Energy Rev.* **2008**, *12*, 1909−1927.
(6) Schlapbach, L.; Züttel, A. Hydrogen-storage materials for mobile applications. *Nature* **2001**, *414*, 353−358.
(7) Hirscher, M. Storage of Hydrogen in the Pure Form. *Handbook of Hydrogen Storage: New Materials for Future Energy Storage*; Academic Press: Wiley-VCH Verlag GmbH & Co. KGaA, 2010; pp 1−37.
(8) Zhu, Q.-L.; Xu, Q. Liquid organic and inorganic chemical hydrides for high-capacity hydrogen storage. *Energy Environ. Sci.* **2015**, *8*, 478−512.
(9) Grochala, W.; Edwards, P. P. Thermal Decomposition of the Non-Interstitial Hydrides for the Storage and Production of Hydrogen. *Chem. Rev.* **2004**, *104*, 1283−1316.
(10) Sakintuna, B.; Lamaridarkrim, F.; Hirscher, M. Metal hydride materials for solid hydrogen storage: A review. *Int. J. Hydrogen Energy* **2007**, *32*, 1121−1140.
(11) Kim, Y.; Kim, S.-h.; Ham, H. C.; Kim, D. H. Mechanistic insights on aqueous formic acid dehydrogenation over Pd/C catalyst for efficient hydrogen production. *J. Catal.* **2020**, *389*, 506−516.
(12) Liu, J.; Lan, L.; Liu, X.; Yang, X.; Wu, X. Facile synthesis of agglomerated Ag−Pd bimetallic dendrites with performance for hydrogen generation from formic acid. *Int. J. Hydrogen Energy* **2021**, *46*, 6395−6403.
(13) Chen, L.-N.; Hou, K.-P.; Liu, Y.-S.; Qi, Z.-Y.; Zheng, Q.; Lu, Y.-H.; Chen, J.-Y.; Chen, J.-L.; Pao, C.-W.; Wang, S.-B.; Li, Y.-B.; Xie, S.-H.; Liu, F.-D.; Prendergast, D.; Klebanoff, L. E.; Stavila, V.; Allendorf, M. D.; Guo, J.; Zheng, L.-S.; Su, J.; Somorjai, G. A. Efficient Hydrogen Production from Methanol Using a Single-Site $Pt1/CeO_2$ Catalyst. *J. Am. Chem. Soc.* **2019**, *141*, 17995−17999.
(14) Afif, A.; Radenahmad, N.; Cheok, Q.; Shams, S.; Kim, J. H.; Azad, A. K. Ammonia-fed fuel cells: a comprehensive review. *Renewable Sustainable Energy Rev.* **2016**, *60*, 822−835.
(15) Martis, M.; Mori, K.; Fujiwara, K.; Ahn, W.-S.; Yamashita, H. Amine-Functionalized MIL-125 with Imbedded Palladium Nanoparticles as an Efficient Catalyst for Dehydrogenation of Formic Acid at Ambient Temperature. *J. Phys. Chem. C* **2013**, *117*, 22805−22810.
(16) Kadhem, A. A.; Al-Nayili, A. Dehydrogenation of Formic Acid in Liquid Phase over Pd Nanoparticles Supported on Reduced Graphene Oxide Sheets. *Catal. Surv. Asia* **2021**, *25*, 324−333.
(17) He, N.; Li, Z. H. Palladium-atom catalyzed formic acid decomposition and the switch of reaction mechanism with temperature. *Phys. Chem. Chem. Phys.* **2016**, *18*, 10005−10017.
(18) Tedsree, K.; Li, T.; Jones, S.; Chan, C. W. A.; Yu, K. M. K.; Bagot, P. A. J.; Marquis, E. A.; Smith, G. D. W.; Tsang, S. C. E. Hydrogen production from formic acid decomposition at room temperature using a Ag−Pd core−shell nanocatalyst. *Nat. Nanotechnol.* **2011**, *6*, 302−307.
(19) Di, L.; Zhang, J.; Craven, M.; Wang, Y.; Wang, H.; Zhang, X.; Tu, X. Dehydrogenation of formic acid over Pd/C catalysts: insight into the cold plasma treatment. *Catal. Sci. Technol.* **2020**, *10*, 6129−6138.
(20) Zhang, J.; Zhang, X.; Xia, G.; Zhang, Y.; Di, L. Cold plasma for preparation of Pd/C catalysts toward formic acid dehydrogenation: Insight into plasma working gas. *J. Catal.* **2021**, *400*, 338−346.
(21) Santos, J. L.; Megías-Sayago, C.; Ivanova, S.; Centeno, M. Á.; Odriozola, J. A. Functionalized biochars as supports for Pd/C catalysts for efficient hydrogen production from formic acid. *Appl. Catal., B* **2021**, *282*, 119615.
(22) Kim, Y.; Lee, H.; Yang, S.; Lee, J.; Kim, H.; Hwang, S.; Jeon, S. W.; Kim, D. H. Ultrafine Pd nanoparticles on amine-functionalized carbon nanotubes for hydrogen production from formic acid. *J. Catal.* **2021**, *404*, 324−333.
(23) Mori, K.; Dojo, M.; Yamashita, H. Pd and Pd−Ag Nanoparticles within a Macroreticular Basic Resin: An Efficient Catalyst for Hydrogen Production from Formic Acid Decomposition. *ACS Catal.* **2013**, *3*, 1114−1119.
(24) Wang, Z.-L.; Yan, J.-M.; Zhang, Y.-F.; Ping, Y.; Wang, H.-L.; Jiang, Q. Facile synthesis of nitrogen-doped graphene supported AuPd−$CeO_2$ nanocomposites with high-performance for hydrogen generation from formic acid at room temperature. *Nanoscale* **2014**, *6*, 3073−3077.
(25) Yan, J.-M.; Wang, Z.-L.; Gu, L.; Li, S.-J.; Wang, H.-L.; Zheng, W.-T.; Jiang, Q. AuPd−MnOx/MOF−Graphene: An Efficient Catalyst for Hydrogen Production from Formic Acid at Room Temperature. *Adv. Energy Mater.* **2015**, *5*, 1500107.
(26) Wang, W.; He, T.; Liu, X.; He, W.; Cong, H.; Shen, Y.; Yan, L.; Zhang, X.; Zhang, J.; Zhou, X. Highly Active Carbon Supported Pd−Ag Nanofacets Catalysts for Hydrogen Production from HCOOH. *ACS Appl. Mater. Interfaces* **2016**, *8*, 20839−20848.
(27) Zhao, X.; Xu, D.; Liu, K.; Dai, P.; Gao, J. Remarkable enhancement of PdAg/rGO catalyst activity for formic acid dehydrogenation by facile boron-doping through $NaBH_4$ reduction. *Appl. Surf. Sci.* **2020**, *512*, 145746.
(28) Ding, R.-d.; Li, D.-d.; Li, Y.-l.; Yu, J.-h.; Jia, M.-j.; Xu, J.-q. Bimetallic PdAu Nanoparticles in Amine-Containing Metal−Organic Framework UiO-66 for Catalytic Dehydrogenation of Formic Acid. *ACS Appl. Nano Mater.* **2021**, *4*, 4632−4641.
(29) Navlani-García, M.; Salinas-Torres, D.; Mori, K.; Kuwahara, Y.; Yamashita, H. Enhanced formic acid dehydrogenation by the synergistic alloying effect of PdCo catalysts supported on graphitic carbon nitride. *Int. J. Hydrogen Energy* **2019**, *44*, 28483−28493.
(30) Yurderi, M.; Bulut, A.; Zahmakiran, M.; Kaya, M. Carbon supported trimetallic PdNiAg nanoparticles as highly active, selective and reusable catalyst in the formic acid decomposition. *Appl. Catal., B* **2014**, *160*−*161*, 514−524.
(31) Mori, K.; Tanaka, H.; Dojo, M.; Yoshizawa, K.; Yamashita, H. Synergic Catalysis of PdCu Alloy Nanoparticles within a Macroreticular Basic Resin for Hydrogen Production from Formic Acid. *Chem.—Eur. J.* **2015**, *21*, 12085−12092.
(32) Peng, W.; Liu, S.; Li, X.; Feng, G.; Xia, J.; Lu, Z.-H. Robust hydrogen production from HCOOH over amino-modified KIT-6-confined PdIr alloy nanoparticles. *Chin. Chem. Lett.* **2022**, *33*, 1403.
(33) Luo, Y.; Yang, Q.; Nie, W.; Yao, Q.; Zhang, Z.; Lu, Z.-H. Anchoring IrPdAu Nanoparticles on $NH_2$-SBA-15 for Fast Hydrogen Production from Formic Acid at Room Temperature. *ACS Appl. Mater. Interfaces* **2020**, *12*, 8082−8090.
(34) Wang, Z.-L.; Yan, J.-M.; Ping, Y.; Wang, H.-L.; Zheng, W.-T.; Jiang, Q. An Efficient CoAuPd/C Catalyst for Hydrogen Generation from Formic Acid at Room Temperature. *Angew. Chem., Int. Ed.* **2013**, *52*, 4406−4409.
(35) Sanchez, F.; Motta, D.; Bocelli, L.; Albonetti, S.; Roldan, A.; Hammond, C.; Villa, A.; Dimitratos, N. Investigation of the Catalytic Performance of Pd/CNFs for Hydrogen Evolution from Additive-Free Formic Acid Decomposition. *C* **2018**, *4*, 26.
(36) Hu, C.; Pulleri, J. K.; Ting, S.-W.; Chan, K.-Y. Activity of Pd/C for hydrogen generation in aqueous formic acid solution. *Int. J. Hydrogen Energy* **2014**, *39*, 381−390.
(37) Gao, Y.; Hu, E.; Yin, G.; Huang, Z. Pd nanoparticles supported on CeO2 nanospheres as efficient catalysts for dehydrogenation from additive-free formic acid at low temperature. *Fuel* **2021**, *302*, 121142.
(38) Jeon, H.-j.; Chung, Y.-M. Hydrogen production from formic acid dehydrogenation over Pd/C catalysts: Effect of metal and


https://doi.org/10.1021/acsomega.2c00601
*ACS Omega* 2022, 7, 14944−14951

support properties on the catalytic performance. *Appl. Catal., B* **2017**, *210*, 212−222.
(39) Jeon, M.; Han, D. J.; Lee, K.-S.; Choi, S. H.; Han, J.; Nam, S. W.; Jang, S. C.; Park, H. S.; Yoon, C. W. Electronically modified Pd catalysts supported on N-doped carbon for the dehydrogenation of formic acid. *Int. J. Hydrogen Energy* **2016**, *41*, 15453−15461.
(40) Koh, K.; Jeon, M.; Yoon, C. W.; Asefa, T. Formic acid dehydrogenation over Pd NPs supported on amine-functionalized SBA-15 catalysts: structure−activity relationships. *J. Mater. Chem. A* **2017**, *5*, 16150−16161.
(41) Zhao, Z.; Heck, K. N.; Limpornpipat, P.; Qian, H.; Miller, J. T.; Wong, M. S. Hydrogen-generating behavior of Pd-decorated gold nanoparticles via formic acid decomposition. *Catal. Today* **2019**, *330*, 24−31.
(42) Lee, J. H.; Ryu, J.; Kim, J. Y.; Nam, S.-W.; Han, J. H.; Lim, T.-H.; Gautam, S.; Chae, K. H.; Yoon, C. W. Carbon dioxide mediated, reversible chemical hydrogen storage using a Pd nanocatalyst supported on mesoporous graphitic carbon nitride. *J. Mater. Chem. A* **2014**, *2*, 9490−9495.
(43) Bi, Q.-Y.; Lin, J.-D.; Liu, Y.-M.; He, H.-Y.; Huang, F.-Q.; Cao, Y. Dehydrogenation of Formic Acid at Room Temperature: Boosting Palladium Nanoparticle Efficiency by Coupling with Pyridinic-Nitrogen-Doped Carbon. *Angew. Chem., Int. Ed.* **2016**, *55*, 11849−11853.
(44) Luo, Y.-X.; Nie, W.; Ding, Y.; Yao, Q.; Feng, G.; Lu, Z.-H. Robust Hydrogen Production from Additive-Free Formic Acid via Mesoporous Silica-Confined Pd-ZrO2 Nanoparticles at Room Temperature. *ACS Appl. Energy Mater.* **2021**, *4*, 4945−4954.
(45) Santos, J. L.; Megías-Sayago, C.; Ivanova, S.; Centeno, M. Á.; Odriozola, J. A. Structure-sensitivity of formic acid dehydrogenation reaction over additive-free Pd NPs supported on activated carbon. *Chem. Eng. J.* **2021**, *420*, 127641.
(46) Navlani-García, M.; Martis, M.; Lozano-Castello, D.; Cazorla-Amorós, D.; Mori, K.; Yamashita, H. Investigation of Pd nanoparticles supported on zeolites for hydrogen production from formic acid dehydrogenation. *Catal. Sci. Technol.* **2015**, *5*, 364−371.
(47) Zhou, X.; Huang, Y.; Xing, W.; Liu, C.; Liao, J.; Lu, T. High-quality hydrogen from the catalyzed decomposition of formic acid by Pd−Au/C and Pd−Ag/C. *Chem. Commun.* **2008**, *30*, 3540−3542.
(48) Song, F.-Z.; Zhu, Q.-L.; Tsumori, N.; Xu, Q. Diamine-Alkalized Reduced Graphene Oxide: Immobilization of Sub-2 nm Palladium Nanoparticles and Optimization of Catalytic Activity for Dehydrogenation of Formic Acid. *ACS Catal.* **2015**, *5*, 5141−5144.
(49) Qin, X.; Li, H.; Xie, S.; Li, K.; Jiang, T.; Ma, X.-Y.; Jiang, K.; Zhang, Q.; Terasaki, O.; Wu, Z.; Cai, W.-B. Mechanistic Analysis-Guided Pd-Based Catalysts for Efficient Hydrogen Production from Formic Acid Dehydrogenation. *ACS Catal.* **2020**, *10*, 3921−3932.
(50) Cho, J.; Lee, S.; Yoon, S. P.; Han, J.; Nam, S. W.; Lee, K.-Y.; Ham, H. C. Role of Heteronuclear Interactions in Selective H2 Formation from HCOOH Decomposition on Bimetallic Pd/M (M = Late Transition FCC Metal) Catalysts. *ACS Catal.* **2017**, *7*, 2553−2562.


https://doi.org/10.1021/acsomega.2c00601
*ACS Omega* 2022, 7, 14944−14951